NUMERICAL STUDIES ON A PIECEWISE SMOOTH VIBRO-IMPACT SYSTEM IN PARAMETERS-STATE SPACES

by

Xianfeng LI[a*], Zhe YANG[a], Guofeng MA[b], and Hui ZHANG[c]

[a]Department of Mathematics, Lanzhou Jiaotong University, Lanzhou, China
[b]Jinchuan Group Company, Jinchang, China
[c]School of Mechanical Engineering, Lanzhou Jiaotong University, Lanzhou, China

Original scientific paper
https://doi.org/10.2298/TSCI2602137L

The present paper is devoted to the synthesis of Poincare mapping and global dynamics of a class of piecewise smooth vibro-impact systems with preloading. The periodic motions are identified numerically in bi-parameter planes. The transition law and the motion pattern are presented as island-like periodic windows. The coexistence of attractors and their basins of attraction in the state planes is then given by cell-to-cell mappings. The numerical results indicate that new attractors can be induced by boundary crises and grazing bifurcations. In the final analysis, the coexisting attractors in disparate regions of bi-parameter planes are subjected to numerical simulation in the joint parameter-state space. It offers a novel approach to the study of the global dynamics of piecewise smooth systems.

Key words: *piecewise smooth, global dynamics, basins of attraction, parameter-state space*

Introduction

Non-smooth systems are ubiquitous in mechanical and electrical systems. The presence of gaps, elastic collisions, and other discontinuous factors leads to a distinct and non--smooth dynamical behavior that differs significantly from that observed in smooth systems. The piecewise smooth vibro-impact systems with preloading are regarded as a distinct non--smooth system, characterized by more intricate and nuanced dynamics. The preload force is modulated by manipulating the compression of a linear spring through the use of bolts and other fasteners. The incorporation of a preload spring enhances the system's discontinuity, thereby resulting in a manifold effect [1]. To study the various non-smooth dynamics and their generation mechanism, a systematic method on grazing bifurcation and concomitant bifurcations in piecewise smooth and rigid-collision systems was given by Nordmark last century [2]. As previously referenced, in their study, Ma *et al.* [3] examined the characteristics of the standard type of the 2-D Poincare mapping of a system with a pre-tensioned spring at the support pads. It was demonstrated that, within this system, the boundary impact bifurcation event occurs concurrently with the observation of an unaltered determinant of the Jacobi matrix, while its trace on the periphery of the boundary converges to an infinite value. An experimental investigation was conducted in [4]. In the fourth section, a generalized vibro-impact system with bidirectional drift is employed through an experimental platform. The text also

* Corresponding author, e-mail: lixf@lzjtu.edu.cn

engaged in a discussion of the dynamic response of systems with different excitation frequencies and amplitudes. Peng *et al.* [5] conducted a study on a 2-DoF friction oscillator with elastic impact and rigid impact on different sides. The study utilized the flow switching theory of discontinuous dynamic systems. Wang *et al.* [6] proposed a novel technique to study the global properties of the vibro-impact system at the impact instant. The 1-D piecewise smooth dynamical systems also garnered significant interest. A general single-DoF vibro-impact system with symmetric and asymmetric constraints was identified and studied [7, 8]. In recent years, considerable research has been dedicated to the vibro-impact system. In order to achieve this objective, analytical and numerical methods were developed that were more effective in their capacity to identify the system's stable periodic orbit, bifurcation, chaotic behavior, grazing dynamics, and stability. These studies have investigated a range of dynamic phenomena, including quasiperiodic chaos, chaos control, and global dynamics, under varying contact laws [9-13]. As indicated by the references listed in the range of [14-23], a wide array of subjects pertaining to non-smooth dynamical systems is encompassed. In order to provide a representative sample, the following subjects are listed, although this list is by no means exhaustive: composite Poincare mapping of double grazing, global dynamics of a harmonically excited oscillator with symmetric constraints, global behavior of a vibro-impact system with asymmetric clearances, analysis of chaotic saddles in a non-linear vibro-impact system, and so on. These investigations provide profound insights and examinations into the dynamic attributes and global behavior of vibro-impact systems.

This paper proposes a novel approach to the study of the global dynamics of piecewise smooth systems. The present study is devoted to the synthesis of Poincare mapping and global dynamics of a class of piecewise smooth vibro-impact systems with preloading. Distinguished coexisting attractors in disparate regions are subjected to numerical simulation within the joint parameter-state space.

The model and its Poincare section

Figure 1 depicts a single-DoF piecewise smooth system with gap and preload, in which the oscillator with mass, M, is connected by a linear spring with stiffness K_1, and a linear damper with damping coefficient, C_1. It is driven by simple harmonic excitation force $F_m\sin(\Omega T + \tau)$ and vibrates back and forth along the horizontal direction. A co-ordinate system is established with the static equilibrium position of the system as the origin of the spatial co-ordinates. The displacement of M is X, and an elastic constraint with the stiffness K_2 is fixed at the distance B on the left side of M. The right side is connected to a linear spring with the damping coefficient, C_1. On the right side of M, an elastic constraint with stiffness, M, and damping coefficient, C_2, is fixed at the position of distance, B, with pre-compression, D. With the simple harmonic excitation, the displacement of M is small, such that the system is linear with one degree of freedom. When the displacement of M is less than $-B$ or more than B, the mass M will vibrate with the elastic constraints on both sides.

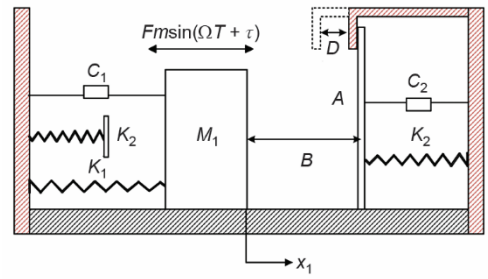

Figure 1. Piecewise smooth collision vibration system

The dimensionless differentl equations of the system is:

$$\begin{gathered}\ddot{x}+2\zeta\dot{x}+x=\sin(\omega t+\tau), \quad -b\le x\le b\\ \ddot{x}+2\zeta(1+\mu_r)\dot{x}+(1+\mu_k)x=\sin(\omega t+\tau)+\mu_k(b-d), \quad x>b\\ \ddot{x}+2\zeta\dot{x}+(1+\mu_k)x=\sin(\omega t+\tau)+\mu_k b, \quad x<-b\end{gathered} \tag{1}$$

in which, the dimensionless parameters are:

$$t=T\sqrt{\frac{K_1}{M}}, \quad x=\frac{K_1X}{F_m}, \quad \zeta=\frac{R_1}{2\sqrt{K_1M_1}}, \quad \omega=\Omega\sqrt{\frac{M}{K_1}}, \quad \mu_r=\frac{C_2}{C_1}$$

$$\mu_k=\frac{K_2}{K_1}, \quad b=\frac{K_1B}{F_m}, \quad d=\frac{K_1D}{F_m}$$

The general solution of the equations is:

$$\begin{gathered}x(t)=e^{-\eta(t-t_1)}\{a_2\cos[\omega_{d2}(t-t_1)]+b_2\sin[\omega_{d2}(t-t_1)]\}+\\ +A_2\cos(\omega t+\tau_0)+B_2\sin(\omega t+\tau_0)+\mu_k(b-d), \ x>b\\ x(t)=e^{-\zeta(t-t_0)}\{a_1\cos[\omega_{d1}(t-t_0)]+b_1\sin[\omega_{d1}(t-t_0)]\}+\\ +A_1\cos(\omega t+\tau_0)+B_1\sin(\omega t+\tau_0), \ -b\le x\le b\\ x(t)=e^{-\zeta(t-t_2)}\{a_3\cos[\omega_{d3}(t-t_2)]+b_3\sin[\omega_{d3}(t-t_2)]\}+\\ +A_3\cos(\omega t+\tau_0)+B_3\sin(\omega t+\tau_0)+\mu_k b, \ x<-b\end{gathered} \tag{2}$$

where

$$\eta=\zeta(1+\mu_r), \quad \omega_{d1}=\sqrt{1-\zeta^2}, \quad \omega_{d2}=\sqrt{(1+\mu_k)-\zeta^2(1+\mu_r)^2}, \quad \omega_{d3}=\sqrt{(1+\mu_k)-\zeta^2}$$

The coefficients a_1, a_2, a_3, b_1, b_2, and b_3 are the integration constants, which are determined by the initial conditions of the system. The A_1, A_2, A_3, B_1, B_2, and B_3 are the amplitude constants, specifically:

$$A_1=\frac{(1-\omega^2)}{(1-\omega^2)^2+4\zeta^2\omega^2}, \quad B_1=\frac{-2\zeta\omega}{(1-\omega^2)^2+4\zeta^2\omega^2}, \quad A_2=\frac{1+\mu_k-\omega^2}{(1+\mu_k-\omega^2)^2+4\zeta^2(1+\mu_r)^2\omega^2}$$

$$B_2=\frac{-2(1+\mu_r)\zeta\omega}{(1+\mu_k-\omega^2)^2+4\zeta^2(1+\mu_r)^2\omega^2}, \quad A_3=\frac{1+\mu_k-\omega^2}{(1+\mu_k-\omega^2)^2+4\zeta^2\omega^2}$$

$$B_3=\frac{-2(1+\mu_r)\zeta\omega}{(1+\mu_k-\omega^2)^2+4\zeta^2\omega^2}$$

To study the stability of the periodic motions on the coexisting regions and to carry out a global dynamics analysis, the following Poincare sections are needed:

$$\begin{gathered}\sum\nolimits_n=\{(x,\dot{x},\theta)\in\mathbb{R}^2\times\mathbb{S}^1, \quad \theta=\mathrm{mod}(\omega t,2\pi/\omega)\\ \sum\nolimits_p=\{(x,\dot{x},\theta)\in\mathbb{R}^2\times\mathbb{S}^1, \quad x=b,\dot{x}>0\\ \sum\nolimits_q=\{(x,\dot{x},\theta)\in\mathbb{R}^2\times\mathbb{S}^1, \quad x=-b,\dot{x}<0\end{gathered} \tag{3}$$

It is convenient to select the orientation surfaces on Σ_n to count the number of cycles of the system periodic motions, while the selections on the Σ_p or Σ_q will benefit for counting the number of collisions to the right and left constraint surfaces.

The schematic diagram of the Poincare mappings is presented in fig. 2. The Poincare mapping is divided into four stages using the two constraint surfaces as boundaries:

$$\begin{aligned} p_1 &: [\dot{x}_-(t_{1-}), \tau(t_{1+})] \mapsto [\dot{x}_+(t_{2+}), \tau(t_{2-})] \\ p_2 &: [\dot{x}_+(t_{2-}), \tau(t_{2+})] \mapsto [\dot{x}_-(t_{3-}), \tau(t_{3+})] \\ p_3 &: [\dot{x}_-(t_{3-}), \tau(t_{3+})] \mapsto [\dot{x}_+(t_{4+}), \tau(t_{4-})] \\ p_4 &: [\dot{x}_+(t_{4+}), \tau(t_{4-})] \mapsto [\dot{x}_-(t_{1-}), \tau(t_{1+})] \end{aligned} \tag{4}$$

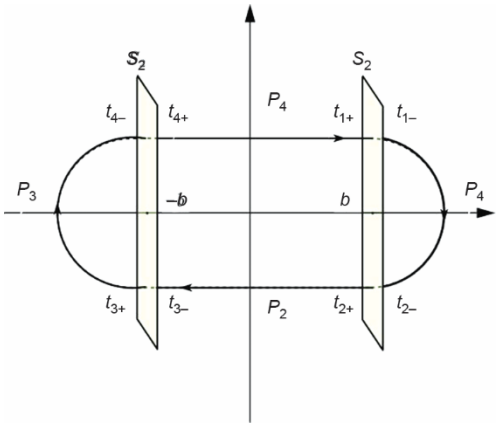

Figure 2. The Poincare mappings

where, noted as more specially, P_1: before the contact of the mass block with the right pre-tensioned constraint to after disengagement, P_2: after disengagement of the mass block from the right pre-tensioned constraint surface to before contact with the left constraint, P_3: the mass block before contact with the left side constraint to after disengagement, and P_4: after disengagement of the mass block from the left side constraint to before contact with the right side pre-tensioned constraint.

Numerical simulations on the parameter space

There are six system parameters, namely, excitation frequency, ω, pre-compression, d, clearance, b, damping coefficient, ζ, damping ratio, μ_r, stiffness coefficient μ_k. Three initial state parameters $x_{10}, \dot{x}_{10}$, and τ_{10} are considered in the following. The system dynamics will be revealed on the parameter plane $\omega - d$ and the system state plane $\tau - \dot{x}$, respectively.

The selected parameter regions are $1.35 \le \omega \le 1.65$, $0.01 \le d \le 0.05$, while fixing other parameters $\zeta = 0.2$, $\mu_r = 0.1$, $b = 0.1$, and $\mu_k = 20$. The periodic orbits and chaotic dynamics are depicted on the parameter plane $\omega - d$ with initial values $\tau_{10} = 0.3$ and $\dot{v}_{10} = 0.1$, as shown in fig. 3. Different colors correspond to the symbols in the figure represent the existence region of the periodic motion. The transmigration law $n/p/q$, is introduced to facilitate the subsequent analysis. Here n is the number of cycles of the periodic motion, p – the number of collisions with the right constraints, and q – the number of collisions with the left constraint surfaces. In the upper right corner of fig. 3(a), there is a fundamental shock vibration 1/2/1. When the excitation frequency, ω, decreases, the period-doubling boundary PB1 splits the plane into two parts. A sequence of period-doubling bifurcations occurs in the left part. The system bifurcates doubly in sequence 1/2/1, 2/4/2, 4/8/4, …, and finally steps into chaos. As the number of multiplicative bifurcations increases the area occupied by each periodic motion decreases. Most of the left region is dominated by white chaotic motion (chaos), but part of the region is sensitive to the change of system parameters, and an island-shaped periodic window appears from the chaotic boundary. In the island-shaped periodic window

(ω, d) ∈ [1.35, 1.37][0.045, 0.05], there is a band of transient periodic orbits due to the period-doubling bifurcations. In the below region after PB1, complex periodic motion patterns and transmigration features appear. The result shown on the magnification fig. 3(b), clearly shows that the process of transmigration of 1/2/1 periodic motion through the grazing bifurcation (GR), the period-doubling bifurcation (PB), and the periodic windows appearing from the chaotic boundary (SB) to various types of periodic motions and chaotic. The specific bifurcation transition laws are given explicitly by the single parameter bifurcation diagrams, as shown in fig. 4(a) and its part magnification fig. 4(b). However, the bifurcation structures are very different with multi setting on the initial values, see the comparison with fig. 3(c), which will be illustrated in great detail soon.

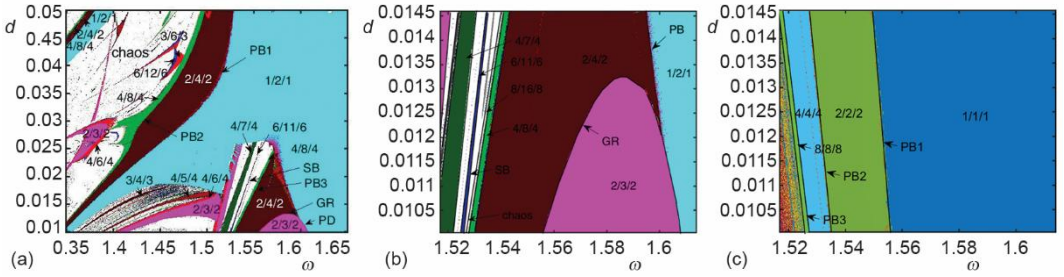

Figure 3. The bifurcation structure on the parameter plane $\omega - d$; (a) the bifurcations and their transients, (b) part of magnification, and (c) $\tau_{10} = 4.1$, $\dot{v}_{10} = 0.2$

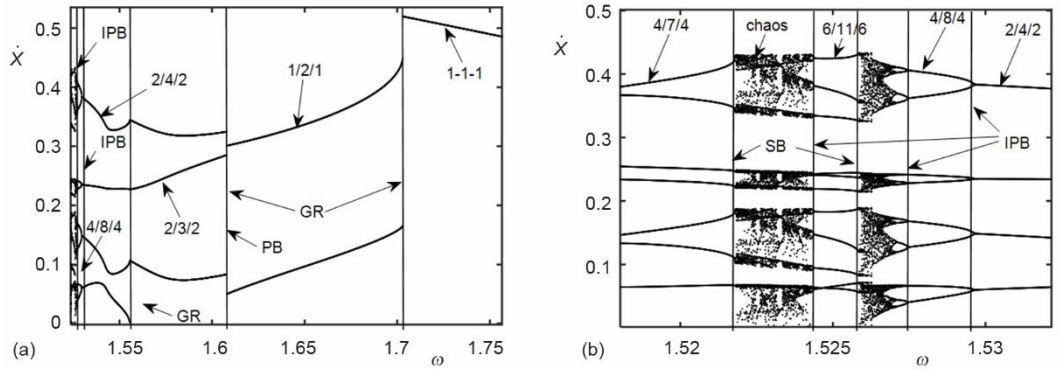

Figure 4. The bifurcation diagram of the system against ω; (a) ω ∈ [1.518, 1.75] and (b) ω ∈ [1.518, 1.533]

In fig. 4(a), the local bifurcation diagram against $\omega \in [1.5, 1.75]$ shows the path to chaos as the excitation frequency, ω, decreases. The system is a stable 1/1/1 cycle. As ω decreases the 1/1/1 cycle is shifted to 1/2/1 after the grazing bifurcation, and then 2/3/2. More details are shown in the phase diagrams fig. 5, which illustrate the shifts of periodic orbits before and after the grazing bifurcation. At the grazing bifurcation, the mass, M, touches the right elastic constraint surface with zero velocity. After that, it follows the period-doubling sequence after another grazing bifurcation about $\omega \approx 1.552$. The successiveness of grazing bifurcations is interrupted by period-doubling bifurcation scenarios before the coming of chaos.

The scenarios start from a 2/4/2, and then goes into 4/8/4, 8/16/8, ... In the magnification figure, fig. 4(b) shows periodic windows induced by saddle-node bifurcations sandwiching in the chaotic regions. The transition law is described:

$$\omega\downarrow: 4/7/4 \xleftarrow{SB} \text{chaos} \xleftarrow{PB} \cdots \xleftarrow{PB} 6/11/6 \xleftarrow{SB} \text{chaos} \xleftarrow{PB} \cdots$$

$$4/8/4 \xleftarrow{PB} 2/4/2 \xleftarrow{GR} 2/3/2 \xleftarrow{GR/PB} 1/2/1 \xleftarrow{GR} 1/1/1$$

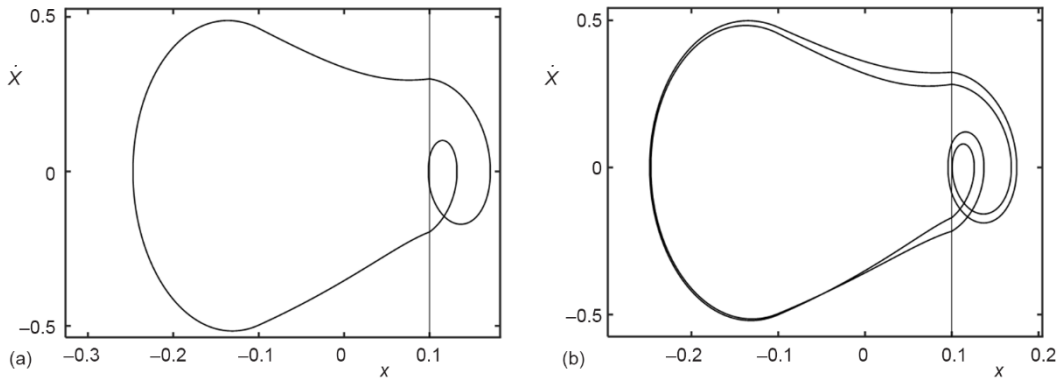

Figure 5. Phase diagrams of periodic orbits before and after the grazing bifurcation; (a) ω = 1.608 period-1 and (b) ω = 1.61 period-2

Numerical simulations on the parameter space

In the following studies, parameters $\zeta = 0.2$, $\mu_r = 0.1$, $b = 0.1$, $\mu_k = 20$, and $d = 0.01$. A section of the local bifurcation superposition diagram against $\omega \in [1.5, 1.75]$ are presented in fig. 6. The bifurcation curves A_i, i = 1, 2, 3, 4 of coexisting attractors with same state parameters, are dotted with different colors.

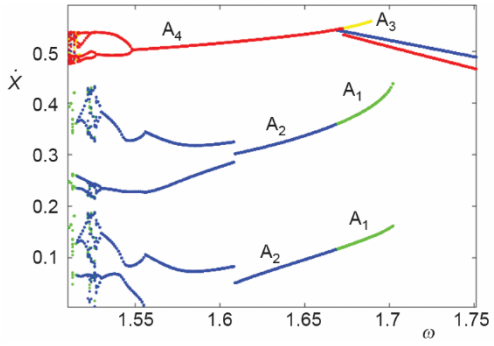

Figure 6. Coexisting attractors

The phase plane:

$$\sigma_p = \{(\tau, \dot{x}) \in \mathbb{R}^2 \mid 0 \le \tau \le 2\pi, 0 \le \dot{x} \le 1.5\}$$

is divided into 1492 × 1750 state cells. And the cells are mapped to the phase plane. The global dynamics of the system with the excitation frequency, ω, are shown in figs. 7(a)-7(f), in which different colors indicate different basins of attraction. Different coexisting attractors are also labelled.

As illustrated in fig. 8, the two-parameter bifurcation charts exhibit distinct initial states for a given set of system parameters. The coexistence of attractors in each region of the 2-D parameter plane is obtained by means of joint simulations. The coexisting attractors in the larger regions are enumerated in tab. 1. This approach is characterized by its enhanced intuitiveness and efficiency in comparison to the previous study of attractor coexistence through

the 1-D system parameter plane. This approach offers a novel methodology for examining the global dynamics of the system.

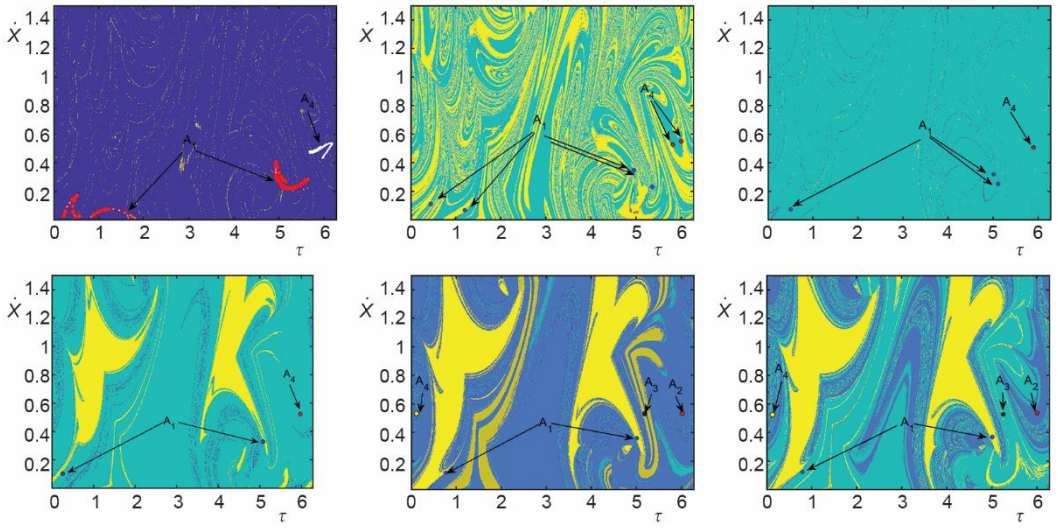

Figure 7. Basins of attraction; (a) ω = 1.5 chaos/chaos, (b) ω = 1.54A_1 (2/4/2)/A_4 (2/2/2), (c) ω = 1.5A_1 (2/3/2)/ A_4 (1/1/1), (d) ω = 1.64A_1 (1/2/1)/ A_4 (1/1/1), (e) ω = 1.67A_1(1/2/1)/A_2(1/1/1), and (f) ω = 1.675A_1 (1/2/1)/A_2 (1/1/1)

Table 1 Coexisting attractor motion patterns

	A1	A4	A1	A4	
S_1	1/2/1	1/1/1	S_2	2/4/2	1/1/1
S_3	2/3/2	1/1/1	S_4	2/4/2	2/2/2
S_5	4/8/4	2/2/2	S_6	chaos	2/2/2
S_7	4/7/4	4/4/4	S_8	4/7/4	chaos
S_9	2/4/2	4/4/4			

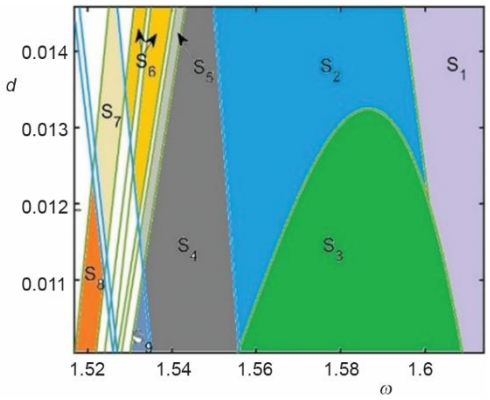

Figure 8. Parameter-state space

Conclusions

In this paper, the authors identify the mode types of periodic motions in the parameter plane of a class of non-smooth collisional vibrating systems with preloading. They establish three Poincare mapping pairs to identify the existence regions and the transitions between neighboring periodic motions. The attraction domains of different attractors and the evolution process of each attraction domain are investigated by using the cell-to-cell mapping method. The coexistence region of different attractors in the system parameter plane is derived by joint simulation of the system parameter-state space. The attractors in piecewise smooth systems

with preloading can be induced by two situations: one is boundary crises, the other is grazing bifurcations. The grazing bifurcation will result in a modification of the attractor's domain structure. The coexistence of different attractors in the 2-D parameter plane can be derived more intuitively through the joint parameter-state space simulation of the system. This approach provides a more efficient method for studying the coexistence of attractors in the global dynamics analysis.

Acknowledgment

The research is supported by the National Natural Science Foundation of China (No. 12462002, No. 11962011), and the Science and Technology Program of Gansu Province (No. 22JR5RA348, No. 20JR10RA223).

References

[1] Laurea, M. di B., *et al.*, *Piecewise-Smooth Dynamical Systems: Theory and Applications,* Springer, New York, USA, 2008
[2] Nordmark, A. B., Non-Periodic Motion Caused by Grazing Incidence in an Impact Oscillator, *Journal of Sound and Vibration, 145* (1991), 2, pp. 279-297
[3] Ma, Y., *et al*., Border Collision Bifurcations in a Soft Impact System, *Physics Letters A, 354* (2006), 4, pp. 281-287
[4] Zhang, J. J., *et al.*, Vibro-Impact Dynamics of an Experimental Rig with Two-Sided Constraint and Bi-directional Drift, *Journal of Sound and Vibration, 571* (2023), 118021
[5] Peng, Y. Y., *et al.*, Discontinuous Dynamics of an Asymmetric 2-DoF Friction Oscillator with Elastic and Rigid Impacts, *Chaos, Solitons and Fractals, 150* (2021), 111195
[6] Wang, B. C., *et al.*, A New Technique for the Global Property of the Vibro-Impact System at the Impact Instant, *International Journal of Nonlinear Mechnics, 14* (2022), 103914
[7] Pourbarat, M., *et al.*, Chaos in One-Dimensional Piecewise Smooth Dynamical Systems, *Journal of Dynamics and Control System, 29* (2023), Jan., pp. 1271-1285
[8] Cao, D. X., *et al.*, Limit Cycle Oscillation and Dynamical Scenarios in Piecewise-smooth Nonlinear Systems with Two-Sided Constraints, *Nonlinear Dynamics, 112* (2024), Apr., pp. 9887-9914
[9] Wu, X., *et al.*, Anti-Controlling Quasi-Periodic Oscillations of Vibro-Impact Systems, *Journal of Vibration Engineering Techniques, 12* (2023), Apr., pp. 1909-1921
[10] Yue, Y., *et al.*, Symmetry Restoring Bifurcations and Quasiperiodic Chaos Induced by a New Intermittency in a Vibro-Impact System, *Chaos, 26* (2016), 113121
[11] Souza, S. L. T., Caldas, I. L., Controlling Chaotic Orbits in Mechanical Systems with Impacts, *Chaos, Solitons and Fractals, 19* (2004), 1, pp. 171-178
[12] Wang, L., *et al.*, The Effect of the Random Parameter on the Basins and Attractors of the Elastic Impact System, *Nonlinear Dynamics, 71* (2013), Nov., pp. 597-602
[13] Gendelman, O., *et al*., Mixed Global Dynamics of Forced Vibro-Impact Oscillator with Coulomb Friction, *Chaos, 29* (2019), 113116
[14] Liu, R., Yue, Y., Composite Poincare Mapping of Double Grazing in Non-Smooth Dynamical Systems: Bifurcations and Insights, *Acta Mechnics Sinica, 234* (2023), June, pp. 4573-4587
[15] Lu, K., *et al.*, Global Dynamics of a Harmonically Excited Oscillator with Symmetric Constraints in Two-Parameter Plane, *Nonlinear Dynamics, 112* (2024), Mar., pp. 8001-8024
[16] Li, G. F., Ding, W. C., Global Behavior of a Vibro-Impact System with Asymmetric Clearances, *Journal of Sound and Vibration, 423* (2018), June, pp. 180-194
[17] Feng, J. Q., Analysis of Chaotic Saddles in a Nonlinear Vibro-Impact System, *Communications in Nonlinear Science and Numerical Simulation, 48* (2017), July, pp. 39-50
[18] Chen, H. B., *et al.*, Global Dynamics of a Mechanical System with Dry Friction, *Journal of Differential Equations, 265* (2018), 11, pp. 5490-5519
[19] Ren, Z., *et al*., Reliability Analysis of Nonlinear Vibro-Impact Systems with Both Randomly Fluctuating Restoring and Damping Terms, *Communications in Nonlinear Science and Numerical Simulation, 82* (2020), 105087
[20] Zhang, H., *et al*., A Calculation Method on Bifurcation and State Parameter Sensitivity Analysis of Piece-Wise Mechanical Systems, *International Journal of Bifurcation and Chaos, 30* (2020), 203003330

[21] Xie, J. H., Ding, W. C., Hopf-Hopf Bifurcation and Invariant Tours T2 of a Vibro-Impact System, *International Journal of Nonlinear Mechnics, 40* (2005), 4, pp. 531-543
[22] Hsu, C. S., Guttalu, R. S., An Unraveling Algorithm for Global Analysis of Dynamical Systems: an Application of Cell-to-Cell Mappings, *Journal of Applied Mechanics, 47* (1980), 4, pp. 940-948
[23] Liu, Y., *et al.*, Vibro-Impact Responses of Capsule System with Various Friction Models, *International Journal of Mechanics, 72* (2013), July, pp. 39-54

Paper submitted: March 2, 2024
Paper revised: May 23, 2025
Paper accepted: May 23, 2025